Continuous structure modification of metal-organic framework glasses via halide salts

Fengming Cao[1,†], Søren S. Sørensen[1,†,], Anders K. R. Christensen[1], Samraj Mollick[1], Xuan Ge[1], Daming Sun[1], Anders B. Nielsen[2,3], Niels Chr. Nielsen[2,3], Peter K. Kristensen[4], Lars R. Jensen[4], Francesco Dallari[5], Jacopo Baglioni[5], Giulio Monaco[5], Martin A. Karlsen[6], Volodymyr Baran[6], Morten M. Smedskjaer[1,*]*

[1]Department of Chemistry and Bioscience, Aalborg University, DK-9220 Aalborg, Denmark

[2]Department of Chemistry, Aarhus University, Aarhus DK-8000, Denmark

[3]Interdisciplinary Nanoscience Center (iNANO), Aarhus University, DK-8000 Aarhus, Denmark

[4]Department of Materials and Production, Aalborg University, Aalborg DK-9220, Denmark

[5]University of Padova, Department of Physics and Astronomy `Galileo Galilei', Via F. Marzolo 8, 35131 Padova, Italy

[6]Deutsches-Elektronen Synchrotron (DESY) Notkestraße 85, 22607, Hamburg, Germany

† These authors contributed equally

* Corresponding Authors.

Emails: Søren S. Sørensen soe@bio.aau.dk; Morten M. Smedskjaer mos@bio.aau.dk

Keywords: Hybrid glasses; metal-organic frameworks; modifier; zeolitic imidazolate frameworks

Abstract

Melting and glass formation of metal-organic frameworks (MOFs) allow them to be processed into bulk materials. However, two major challenges remain: only a small fraction of MOF crystals undergo melting and glass-formation, and no well-established strategies exist for tuning MOF glass structures and properties. Here, we address both challenges through co-melting of zeolitic imidazole frameworks (ZIFs), a subset of MOFs, with heterocycle-based halide salts. The salt acts as a chemical "modifier", akin to the role of alkali modifiers in traditional silicate glasses, allowing the melting of ZIF-8 that otherwise decomposes prior to melting. Through experimental and computational analyses, we show that the salts depolymerize the ZIFs, enabling continuous tuning of the fraction of bridging to non-bridging imidazolate linkers and, thereby, the thermal and mechanical properties. The proposed strategy enables diversification of MOF glass chemistry, tunable structures and properties, and ultimately an increased number of glass-forming MOFs with new functionalities.

Introduction

Inorganic and organic glass materials exhibit remarkable versatility in processing, with their abilities to be shaped into various forms and for their chemical compositions to be continuously tuned[1]. An important family of organic-inorganic hybrid materials, metal-organic frameworks (MOFs), have not yet achieved the same level of processability and continuous composition tunability[2]. MOFs offer exciting prospects for their uses as, e.g., catalysts[3], gas adsorbers[4, 5], and electrolytes[6], especially enabled by their high porosity (surface area up to >10,000 $m^2 g^{-1}$)[4, 7, 8], but their practical applications are often hindered by poor processability as they are typically only available in powder form[9].

The recent discovery of MOF glasses through melting and quenching may help solve this problem as they maintain many properties of the parent MOF crystals while also allowing the processing into grain-boundary-free bulk (>1 cm) objects through hot forming techniques[10]. However, to realize

processable MOFs, a key challenge is to tune the viscosity-temperature curve, which is essential for shaping MOF glasses into desired shapes and configurations, beyond mere melting or sintering techniques[11]. Another significant hurdle is the limited number of meltable MOF crystals, as the melting temperature of many MOFs is higher than their decomposition temperature ($T_m > T_d$)[12]. This restricts the continuous composition tuning of MOF glasses. Currently, the number of known MOF glasses is <200, in stark contrast to the >100,000 known MOF crystals[13, 14]. In comparison, there are more than 200,000 known oxide glass compositions in the SciGlass database, compared to ~70,000 oxide crystals[15]. This difference is ascribed to the inherent feature of oxide glasses to be formed in a nearly infinite number of compositions through mixing of pure glass network formers (SiO_2, GeO_2, B_2O_3, etc.) with so-called 'modifiers' (e.g., alkali, alkaline earth, and transition metal oxides)[16]. These modifiers typically depolymerize the oxide network structure, allowing continuous modification of glass structure and properties. Despite the success of using modifiers in oxide as well as sulfide, fluoride, and chalcogenide glasses[1], no well-established modification platform exists for MOF glasses.

Several families of glass-forming MOFs exist, including zeolitic imidazolate frameworks (ZIFs)[17]. ZIFs feature topologies analogous to those of silica or zeolite networks (Fig. 1a), with tetrahedra consisting of a metal ion (e.g., Co^{2+}, Zn^{2+}) and four imidazolate-based ligands[14, 18]. The first family of MOFs with demonstrated melting behavior was ZIFs and they have since then been the most studied MOF glass family. This includes the discovery of various meltable compositions (e.g., ZIF-4, ZIF-62, and ZIF-76)[19], simulation studies of the bond-breaking behavior leading to melting and glass-formation[20], as well as the effect of pressure on phase transitions[21]. More recent studies have investigated the effect of changing the metal node[22, 23] and organic linker ratio[22], as well as the addition of water[24] and an ionic liquid[12] on various types of hybrid organic-inorganic glasses. In ZIF-62 ($Zn(Im)_{1-x}(bIm)_x$, where Im is imidazolate and bIm is benzimidazolate), changing the linker ratio results in only moderate changes of T_m and T_g (by about 70 and 30 °C, respectively, when x changes from 0.35 to 0.03). Hydrothermal treatment of ZIF-62 glass gives rise to OH^- incorporation and results in larger changes of T_m (from 447 to <300 °C) and T_g (from 320 to ~200 °C)[24]. Another study showed that ionic liquid (1-ethyl-3-methylimidazolium bis(trifluoromethanesulfonyl)imide)

addition enables melting of the otherwise unmeltable ZIF-8 ($Zn(mIm)_2$, where mIm is 2-methylimidazole) crystal, yet with transitions temperatures comparable to those of other meltable ZIFs (T_m≈380 °C and T_g≈320 °C)[12].

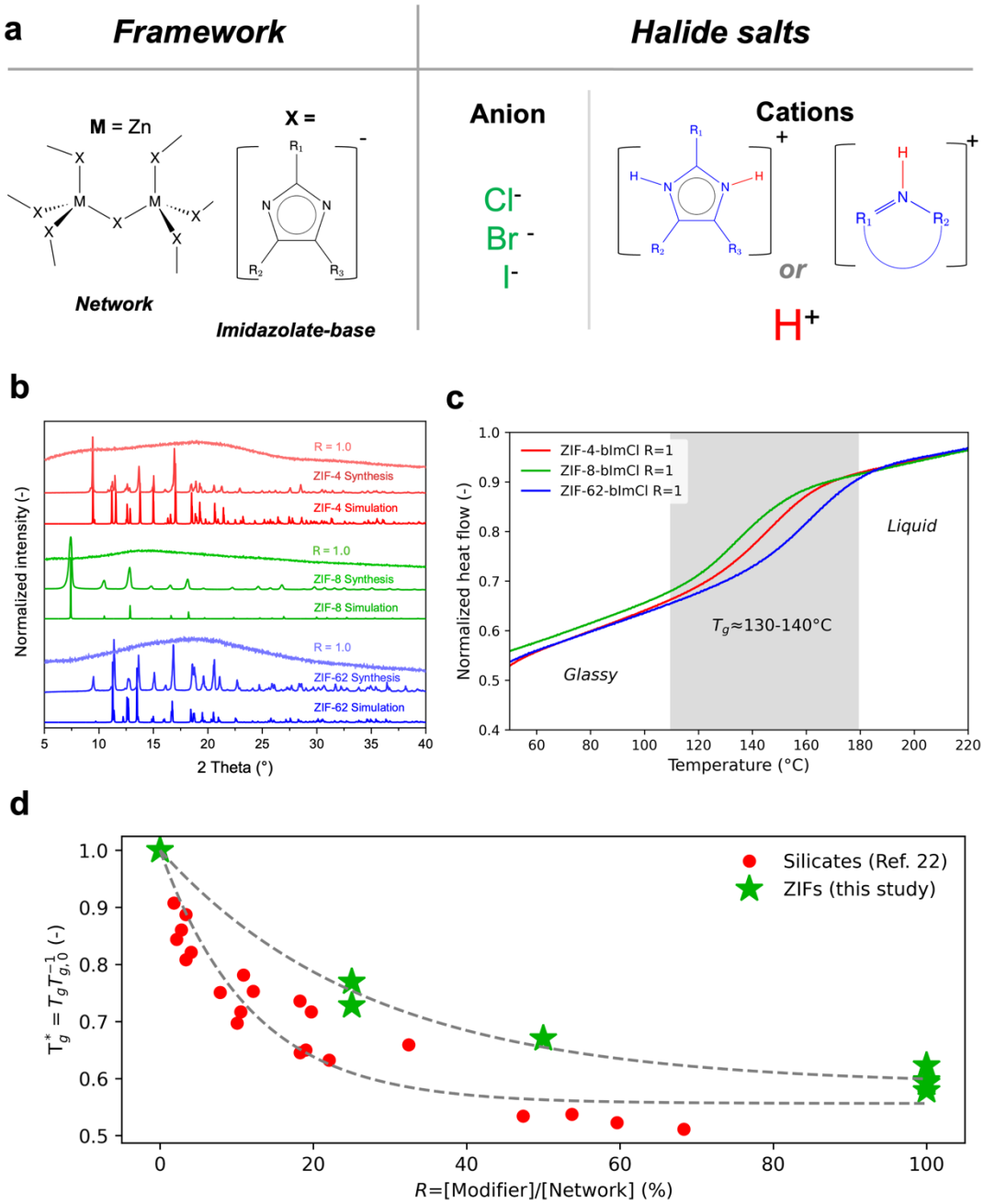

Fig. 1: Structural, crystallographic, and thermal properties of modified zeolitic imidazole frameworks. a, Sketch of polymerized zeolitic imidazole framework and its imidazolate-based linkers (left) and the added halide salts (right). **b,** X-ray diffraction patterns of ZIF-4, ZIF-8, and ZIF-62, including simulated and experimental crystalline forms and experimentally formed glasses

upon co-melting with benzimidazolate chloride (R=1.0). **c,** Fast scanning calorimetry heat flow data of ZIF-4, ZIF-8, and ZIF-62 co-melted with benzimidazolate chloride (R=1.0), showing glass transition temperatures (T_g) in the range of 130-140 °C. The heating rates used for these measurements were 500 K s^{-1}. **d,** Effect of modifier content on the reduced glass transition temperature ($T_g^* = T_g T_{g,0}^{-1}$, where T_g is the glass transition of a modified glass and $T_{g,0}$ is the glass transition temperature of a pure glass former), shown for all modified ZIF-4 and ZIF-62 glasses of the current study (see Supplementary Table 1) as well as literature data for silicates[25]. The dashed lines represent guides for the eye based on exponential decay functions.

The concept we attempt to realize herein is to break up the polymerized ZIF network by introducing new types of bonds in the system. Inspired by the concepts of bridging and non-bridging oxygens in oxide glasses, mixed linker systems in, e.g., oxysulfides and oxynitrides (where oxygen, sulfur, and nitrogen link metal centers)[1], and a crystalline Zn-imidazolate-chloride system[26] (where both imidazole and Cl bond to Zn), we propose a method for modifying ZIF glasses by adding a halide salt. Specifically, we use heterocycle-based halide (Cl, Br, I) salts for co-melting with ZIF crystals, achieving melting below 300 °C, very low T_g values (<150°C), and the preparation of bubble-free bulk-sized samples (>1 cm). We chose these salts as they mimic the linker polarity of the existing framework, and they introduce halide ions, which are known to allow for ligand exchange in ZIF-like networks[27]. Through *ex situ* and *in situ* structural analyses, *ab initio* molecular dynamics simulations, and mechanical and thermal characterization, we conclude that the halide salts act as modifiers in the ZIF network by partially replacing the imidazolium-based organic linkers with the halide anions (Fig. 1a). This method provides a pathway for continuously tuning, e.g., glass transition temperature, mechanics, and chemical durability of MOF glasses, and ultimately a means to increase the diversity of synthesizable MOF glasses.

Result and Discussion

Preparation and thermal properties of modified ZIF glasses

Our study focuses on the well-known ZIF-62 [$Zn(Im)_{1.75}(bIm)_{0.25}$], ZIF-4 [$Zn(Im)_2$], and ZIF-8 [$Zn(mIm)_2$] (where 2-mIm is 2-methylimidazole, see Methods). ZIF-62 and ZIF-4 are known glass-

formers with melting temperatures of 430 and 593 °C, respectively[19]. In contrast, ZIF-8 is known to decompose before melting (T_d~450 °C)[12]. We mix each of these three ZIF crystals with varying amounts (R=0.25, 0.5, 0.75, 1.0) of heterocyclic halide salts (Fig. 1a), where R is the molar ratio between the added amounts of ZIF crystal and modifier salt, i.e., $R=[n_{modifier}]/[n_{ZIF}]$. We note that we mainly investigate the glasses with added benzimidazolium chloride salt for R=1 due to their lower hygroscopicity and thereby easier handling for all testing. However, to demonstrate the universality of our approach, we perform selected thermal, mechanical, and structural analyses for samples with varying R value and halide ion.

Fig. 1b shows the x-ray diffractograms of crystalline ZIF-4, ZIF-8, and ZIF-62 as well as these crystals co-melted with benzimidazolium chloride (bImCl) for R=1.0 at a temperature of 300 °C. All these systems become glassy upon mixing, heating, and quenching. We note how this melting temperature is below that of most other known ZIF systems, for example, ZIF-UC-6[28] [$Zn(Im)_{1.82}$(5-aminobenzimidazole)$_{0.18}$] (T_m=345 °C, T_g=316 °C), which melts at a markedly lower temperature than other Pbca ZIFs, linker-functionalized TIF-4 [Zn-$(Im)_{1.8}$(mbIm-5-methylbenzimidazolate-$C_8H_7N_2)_{0.2}$] (T_m=440 °C, T_g=336 °C), and ZIF-UC-5 [$Zn(Im)_{1.8}$(ClbIm-5-chlorobenzimidazolate-$C_7H_4N_2$-Cl^-))$_{0.2}$] (T_m=428 °C)[29]. After melt-quenching, the recovered samples were subjected to thermal analyses through fast differential scanning calorimetry (FDSC) measurements (Fig.1c). This technique was chosen over traditional DSC because it is less prone to glass relaxation effects and because some of the samples feature weak glass transitions (see Supplementary Text). Using FDSC, we, however, identify clear glass transition temperatures (T_g) for all three ZIFs in the range of 130-140 °C (see Supplementary Table 1), i.e. ~200 °C below that of the T_g of the unmodified glasses in the case of ZIF-4 and ZIF-62 as measured by traditional DSC (note that ZIF-8 does not melt at R=0)[19, 30]. This confirms the formation of glasses for all the co-melted samples.

Addition of modifiers in network glasses, e.g., silicates, is generally associated with depolymerization[1]. This results in a monotonic change of glass properties with the modifier content, such as decreasing T_g with increasing modifier content[1]. To study if this is also the case for the present samples, we have prepared glassy mixtures of each of the three ZIFs co-melted with bImCl

for *R* values of 0.25, 0.5, 0.75, and 1.0. Generally, higher temperatures are required to fully melt the system for lower values of *R* (see XRD results in Supplementary Fig.1), but we note that all samples reach a fully molten state at ~300-360 °C (see photographs of recovered samples in Supplementary Fig. 2). Using FDSC, we find a monotonic decrease in T_g with increasing modifier content, in good resemblance with other network glasses (see comparison of varying *R* on T_g in Fig. 1c,d and raw data in Supplementary Fig. 3 and Table 1). Notably, we observe that the modified glasses are prone to a permanent increase in T_g upon subsequent heating (>300 °C) for few minutes or even seconds (Supplementary Fig. 4). An effect we assign to evaporation of Im and bIm species coming from both the network and added modifier salt (see Supplementary Text). Considering the mechanical properties, the Vicker's hardness of the ZIF-4-bImCl and ZIF-62-bImCl (*R*=1.0) glasses is lower (~0.35 GPa, Supplementary Fig. 5a) than that of the unmodified ZIF glasses (~0.6 GPa)[31, 32]. Similarly, the crack initiation resistance[33] of ZIF-4-bImCl and ZIF-62-bImCl (*R*=1.0) glasses are 0.12 N and 0.38 N, respectively (Supplementary Fig. 5b), significantly lower than that of the unmodified ZIF-62 glass (~2 N)[33].

Photographs and scanning electron micrographs (SEM) of the samples are shown in Fig. 2a,d and Supplementary Fig. 6. The samples are found to take the shape of the container in which they were melted and feature smooth surfaces, indicating viscous flow and a grain-boundary-free glassy state. Furthermore, the modified ZIF-4 and ZIF-62 samples are transparent (see transmission data of ZIF-4-bImCl glass in Supplementary Fig. 7) and we find it possible to produce defect-free samples with size of >1 cm for the modified ZIF-4, ZIF-8, and ZIF-62 glasses (Fig. 2a). This stands in significant contrast to the case of unmodified ZIF-62 and especially unmodified ZIF-4 glass, the quality of which are often impaired by partial decomposition and foaming[10] (Fig. 2b,c). Based on the observed transparency and the compositional analysis performed using energy-dispersive X-ray (EDX) spectroscopy (Fig. 2e and Supplementary Fig. 6), we infer that the samples are homogenous in the elements tested (C, N, Zn, Cl) at both the micro- and macro-scales, although we find depletion of Cl in the ZIF-62-bImCl sample (Supplementary Fig. 6c). In comparison, previous efforts to lower the melting point of ZIF-8 below its decomposition temperature using ionic liquids, which employed melting temperatures around 600 °C, created samples with sizes of <1 mm[12].

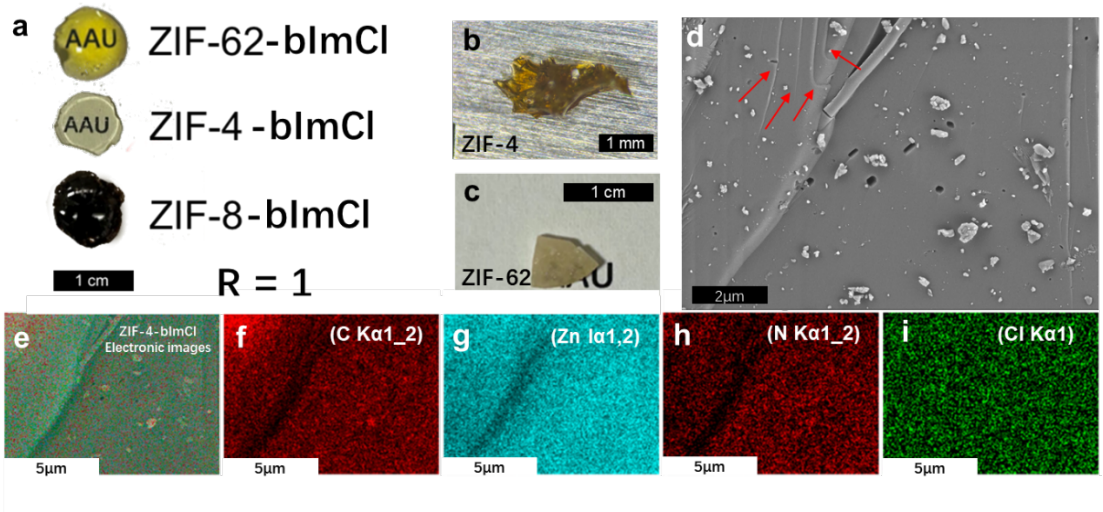

Fig. 2: Photographs and SEM images of bImCl modified ZIF glasses. a, Photographs of bImCl-modified ZIF-4, ZIF-8, and ZIF-62 (R=1) glasses after melt-quenching. Clear transparency is observed for the ZIF-4-bImCl and ZIF-62-bImCl samples. **b,c,** Photographs of unmodified: **b,** ZIF-4 and **c,** ZIF-62 glasses. Note the scale differences in panels **a-c**. **d,e,** SEM images of ZIF-4-bImCl (R=1) glass, showing smooth viscous flow and fracture lines, suggesting the existence of a liquid-like state during forming (red arrows). **f-i,** EDX measurements of ZIF-4-bImCl glass for: **f,** C, **g,** N, **h,** Zn, and **i,** Cl.

In addition to using bImCl as the modifier salt, we also find glass formation upon co-melting the ZIF crystals using benzimidazolium salts with bromide (Br^-) and iodide (I^-) as anions. In summary, we find similar T_g values and loss of crystallinity upon melt-quenching for the Br^- and I^- based salts as for the Cl^- based salts (see XRD and calorimetry data as well as photographs in Supplementary Figs. 8-10), indicating a similar mechanism of ZIF modification.

Structural characterization

Having established the thermodynamical and mechanical characteristics of the modified ZIF glasses, we next investigate their structural features. Notably, two previous studies have solved the single-crystal structure of a bis(imidazole)zinc(II) chloride phase, revealing a mixed linker structure, where each tetrahedral Zn is coordinating two imidazoles and two chloride anions[26, 27]. Another very recent work prepared closely-related bis(benzimidazole)zinc(II) halide (Cl, Br, I) single crystals and

showed that these can be melt-quenched into glasses with T_g values around 80°C[34]. In the following, we demonstrate that the present co-melted ZIF-modifier systems adopt largely similar local configurations, where the Zn nodes coordinate to a mixture of halide anions and imidazolate linkers. However, our approach is fundamentally different in that it does not require the prior preparation of a phase-pure single-crystalline phase, i.e., it is akin to network modification in traditional glasses as the present samples can feature any fraction of bridging to non-bridging imidazolate linkers. Consequently, this enables continuous tuning of both structure and properties in this material family.

We first analyze the synthesized ZIF-4-bImCl, ZIF-62-bImCl, and ZIF-8-bImCl samples (with varying *R*) using FTIR and Raman spectroscopy, revealing that the imidazolate and benzimidazolate linkers remain intact and do not decompose upon melt-quenching (Supplementary Figs. 11-12, Supplementary Table 2, Supplementary Text). We also probe the structure of the modified ZIF glasses (for *R*=1.0 using bImCl) through X-ray photoelectron spectroscopy (XPS, see Supplementary Figs. 13-14) and compare the spectra to those of the unmodified ZIF crystals[35] (noting that the XPS signal of ZIF glasses and crystals are known to be very similar[35]). Upon glass formation, we observe a broadening of the C1s, N1s, and Zn2p peaks as well as an additional shoulder peak in the N1s spectra for all glasses at relatively high energy (~404 eV). We assign the latter to the formation of pyrrolic nitrogen (N bonded to both C and H) upon co-melting with the halide salt, as this species is introduced through the bIm^+ cation in contrast to the lower-energy peak (~402 eV) from pyridinic nitrogen (N bonded to C).

We then characterize the structure of the modified ZIF-62-bImCl (*R*=1.0) glass using high-field solid-state ^{67}Zn, ^{15}N, ^{13}C, and ^{1}H magic-angle spinning (MAS) NMR spectroscopy and compare the results to those of the unmodified ZIF-62 glass[24, 27]. The ^{67}Zn MAS NMR data in Fig. 3a (including a simulated spectrum made using SIMPSON[36]) show a slight change of the chemical shift upon co-melting with the bImCl salt. In comparison to previous ^{67}Zn measurements of ZIF-62 glass (δ_{iso}=278 ppm)[37] and crystalline bis(imidazole)zinc(II) chloride (δ_{iso}=265 ppm)[26], the present glass features a chemical shift of δ_{iso}=268 ppm, indicating a bonding environment very similar to that in bis(imidazole)zinc(II) chloride crystal, i.e., suggesting direct bonding between Zn and Cl^-.

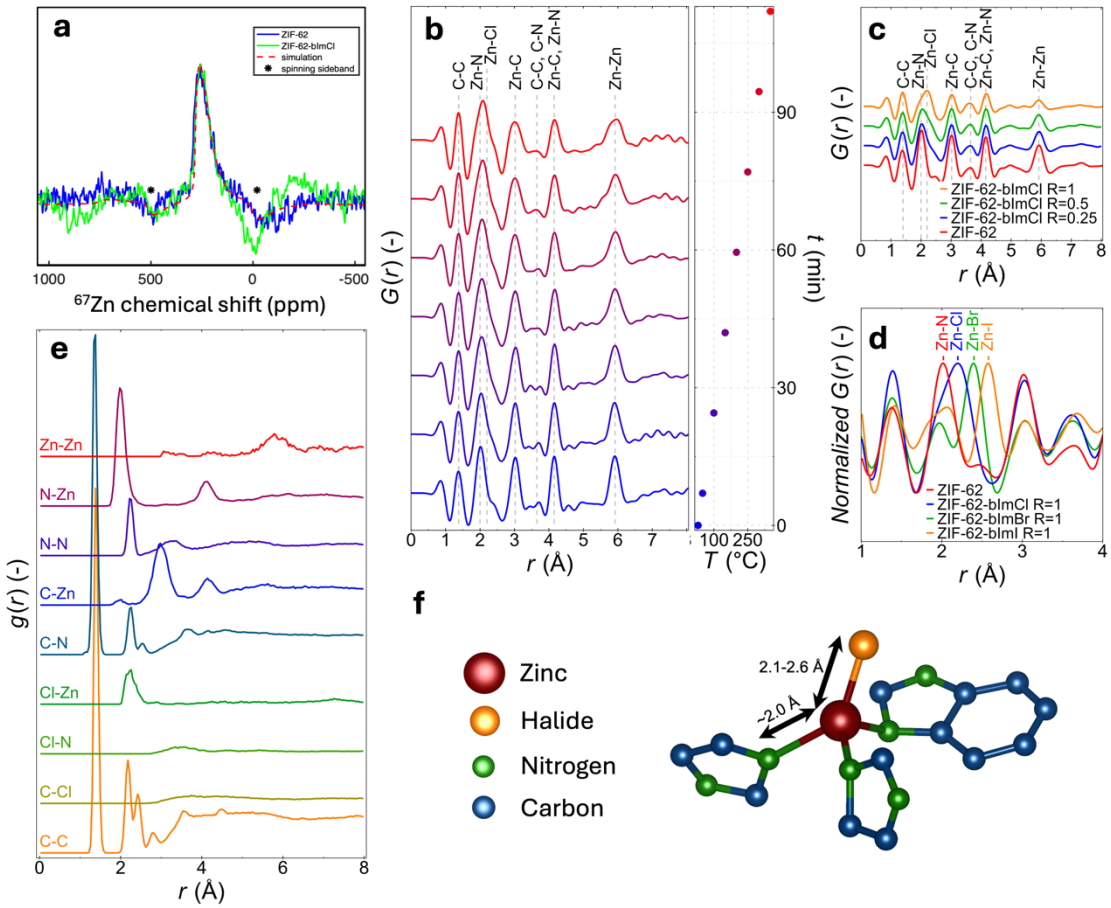

Fig. 3: Structural analysis of modified ZIF glasses using ^{67}Zn solid-state NMR and *in situ* pair distribution function analysis. a, ^{67}Zn MAS NMR spectrum of unmodified ZIF-62 and modified ZIF-62-bImCl (R=1) glasses. Spinning sidebands are denoted with '*'. **b,** *In situ* variable temperature pair distribution function (PDF), $G(r)$, of the ZIF-62-bImCl R=0.5 sample, starting from the mixture of ZIF crystal and chloride salt at time t=0. **c,** PDFs of glassy ZIF-62-bImCl samples with R = 0, 0.25, 0.5, and 1.0 (at room temperature) with assigned peaks. We note how C-C and C-N peaks stem from the internal correlations of both imidazolate and benzimidazolate linkers. **d,** Example of the 1-4 Å region of the PDF (normalized by maximum intensity) of ZIF-62-bImB glasses where B=[Cl, Br, I]. All PDFs shown in panels **c** and **d** have been modified using a Lorch function with Q_{max}=20 Å^{-1}. **e,** Partial PDFs of a simulated structure of ZIF-62-bImCl R=0.5. **f,** Atomic snapshot from first principles simulation of the structure of a Zn tetrahedron where one imidazolate linker is exchanged for a halide.

Furthermore, as shown in Supplementary Figs. 15-17, we find significant changes of the solid-state

^{15}N MAS NMR shifts upon halide salt addition, including the appearance of multiple new peaks, which we assign to non-bridging benzimidazole and imidazole species as introduced from the bImCl salt and the network itself. This is because the two N are not equivalent in the modified ZIF glass structure as one is protonated (δ<180 ppm) while the other is linked to Zn (δ>180 ppm)[38, 39] (see sketches in Supplementary Figs. 15-17). Furthermore, the addition of benzimidazole species through the bImCl salt is clearly seen as an increase in the intensity at δ~190 ppm (Supplementary Fig. 15). Similarly, the solid-state ^{13}C MAS NMR measurements show the enhanced intensity of peaks due to benzimidazole species in the structure (δ~110-130 ppm region in Supplementary Fig. 16). New peaks at δ~135 ppm furthermore indicate the asymmetry of electron density associated with the pure Im and bIm species[40]. The solid-state ^{1}H MAS NMR measurements reveal a broad peak around 5-7 ppm for both ZIF-62 and ZIF-62-bImCl glasses, which we assign to the aromatic proton. Finally, an additional peak at ~12 ppm is observed in the ZIF-62-bImCl glass (Supplementary Fig17), which we ascribe to the N-H proton in pure Im and bIm species[40].

To confirm the presence of mixed organic-halide linkers in the modified ZIF glasses, we have performed *in situ* high temperature X-ray pair distribution function (PDF) measurements of the three crystalline ZIFs mixed with the imidazolium-based halide salts (Cl^-, Br^-, I^-). An example of the recorded pair distribution function, $G(r)$, data is shown in Fig. 3b for the ZIF-62-bImCl (R=0.5) sample heated from room temperature to 300 °C and then cooled back to room temperature. The reciprocal space data (total scattering structure factor, $S(Q)$) are shown in Supplementary Fig. 18, revealing a loss of crystallinity at around ~300 °C, indicating melting at a temperature much lower than the T_m of unmodified ZIF-62 (~450 °C). The PDF data in Fig. 3b mainly show changes in the intensities and shape of the peaks around 2, 4, and 6 Å, which all appear to broaden with increasing temperature.

We also present room temperature PDF data of the melt-quenched ZIF-62-bImCl glasses with R values of 0, 0.25, 0.5, and 1.0 (Fig. 3c). We note that these samples were cooled faster (in our laboratory) than what was possible during the *in situ* PDF experiments at the beamline. We find that the ZIF-62-bImCl glass features both new peaks and differences in peak intensities in comparison

to the unmodified ZIF-62 glass. Notably, the peak at ~2.1 Å broadens and shifts toward a higher interatomic distance, consistent with the expected Zn-Cl bond (~2.2 Å) (see Fig. 3c)[26, 41] compared to the existing Zn-N bond (~2.0 Å)[30]. Similarly, we observe a broadening and decrease of intensity of the peak at ~6 Å, corresponding to the Zn-Zn correlation, thus indicating a reduction in the number of bridging Im species (i.e., Zn-Im-Zn), which we again interpret as being due to the incorporation of Cl. These findings support a mechanism of depolymerization of the ZIF network through partial (benz)imidazolate linker exchange for Cl.

We have also probed the structure of the modified Br^- and I^- analogous glasses (Fig. 3d). We find strong peaks corresponding to the expected bond lengths of Zn-Br (~2.4 Å) and Zn-I bonds (~2.6 Å), supporting the partial (benz)imidazolate for halide exchange[42, 43]. The *in situ* PDF data for these systems show that the Zn-Br and Zn-I bonds are formed upon heating. This is more evident in the Br^- and I^- glasses compared to the Cl^- glass due to the longer bond lengths of Zn-Br and Zn-I compared to Zn-N, while the bond lengths of Zn-Cl and Zn-N are more similar. The appearance of a Zn-halide bond is found in all studied systems containing halide ions as compared to the pure ZIFs (Supplementary Figs. 19-21).This includes ZIF-62-bImCl (with varying *R,* Supplementary Figs. 24-27), ZIF-4-bImCl (Supplementary Fig. 22), and ZIF-8-bImCl (Supplementary Fig. 23), ZIF-62-bImBr (Supplementary Fig. 28), and ZIF-62-bImI (Supplementary Fig. 29). Additionally, these systems exhibit notably varying amorphization/melting temperatures (200-350 °C), decreasing with increasing amount of halide modifier salt. To test the universality of our approach, we have also attempted using imidazolium chloride and pyridinium chloride as modifiers and co-melted these with the different ZIF crystals. We find that these chloride compounds also lead to transparent bulk solids (except for ZIF-4-PyCl, which is transparent but liquid-like). The ZIF-62-ImCl system was also tested by in situ X-ray diffraction as shown in Supplementary Fig. 30. All these samples were found to be non-crystalline (Supplementary Figs. 31-32).

In addition to the above experiments, we have also performed *ab initio* molecular dynamics (AIMD) simulations of the ZIF-62-bImCl R=0.5 system at 1000 K. The simulated system consisted of a single unit cell of crystalline ZIF-62 (296 atoms) mixed with 8 $bImH^+$ and 8 Cl^-. After 10 ps of

simulation, we find an overall decrease in energy (converged after ~6 ps, see Supplementary Fig. 33) and that all 8 Cl^- atoms are coordinated to Zn atoms (bond length of ~2.2 Å), with one case of an imidazolate linker obtaining a hydrogen atom from the added benzimidazolium. Based on this simulation, we show the partial PDFs of the most relevant atomic pair-correlations in Fig. 3e. These results were also used in the assignment the experimental peaks in Fig. 3b,c, confirming that the observed bond lengths correspond very well with newly formed peaks in the ZIF-62-bImCl (R=0.5) glass. Lastly, based on the performed AIMD simulation, we present an example configuration of a Zn node coordinated with a mixture of (benz)imidazolate and chloride (Fig. 3f). Interestingly, in the AIMD simulation, we observe some cases of Zn-Cl-Zn bridges (like the bonding in crystalline $ZnCl_2$). We hypothesize that these may also be formed experimentally upon evaporation of free or non-bridging (benz)imidazole species (as observed experimentally, see Supporting Text). This explains the observed increase in T_g of the modified ZIF glasses upon subsequent annealing (see Supplementary Fig. 5 and Supplementary Text), since the structure should become more rigid when non-bridging imidazolate linkers are replaced by bridging halide species.

Mechanism of ZIF modification

Based on the experimental and simulation data, we propose the ZIF structural modification mechanism shown in Fig. 4, including a comparison to the well-known modification of silicate glasses by alkali modifiers. The polymerized ZIF network consists of zinc metal nodes connected by bridging organic linkers (X). Addition of the modifier halide salt consisting of a proton-containing cation (here, a heterocycle denoted $[H\text{-}A]^+$), which may easily exchange its proton (H^+) together with a halide anion (denoted $[B^-]$), results in a partially depolymerized ZIF network. That is, upon heating, the breaking and reformation of Zn-N coordination bonds lead to changes in the coordination framework. During this process, Zn nodes coordinate to mixed linkers of protonated heterocycles as well as the added halide anions. Continued heating of either the existing liquid or the already-formed glass (below the decomposition temperature) may result in evaporation of the loosely bound heterocycle (denoted as A) as well as the non-bridging X-H species, which leads to re-polymerization of the framework.

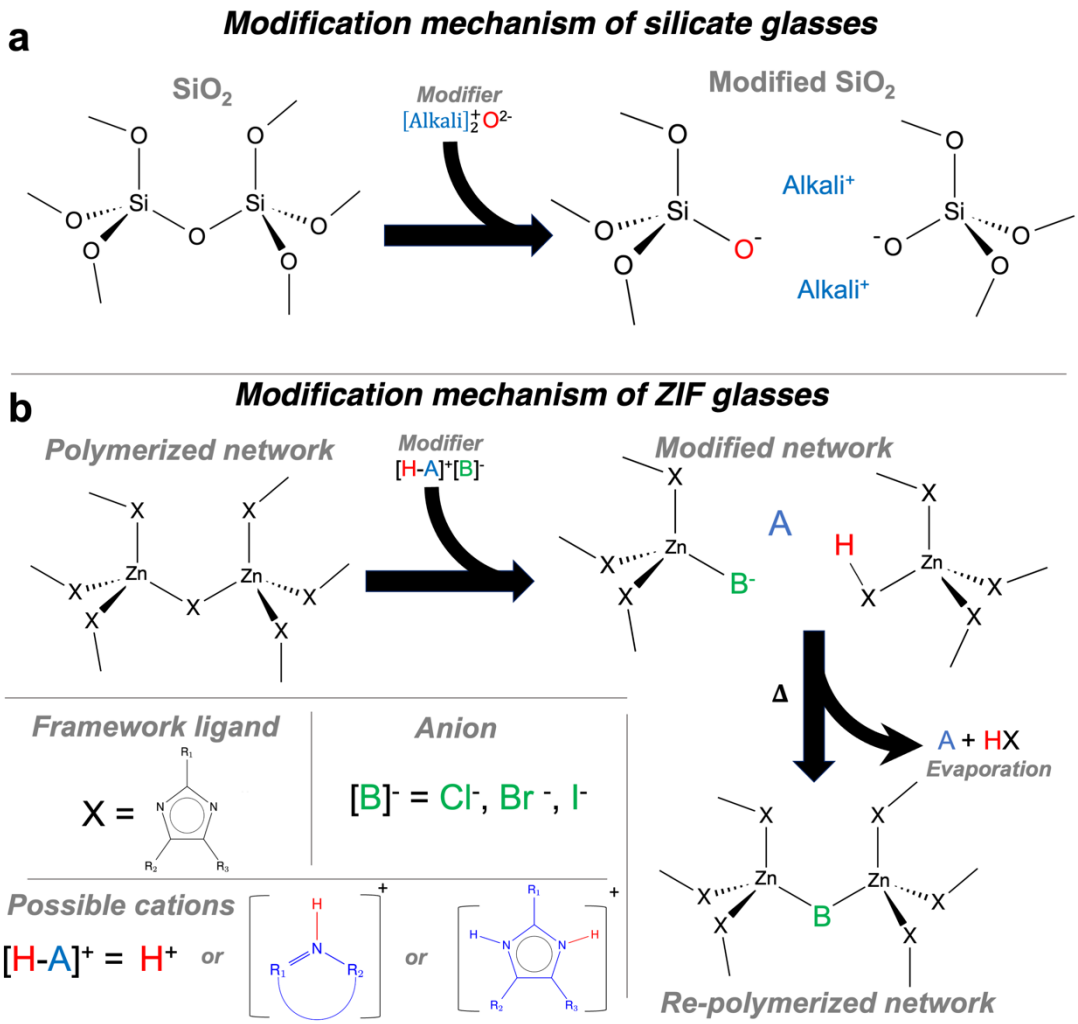

Fig. 4: Proposed mechanism of modification for ZIF glasses using halide salts. a, Well-established mechanism of modification of archetypical silicate glasses using alkali oxides. **b,** Proposed halide salt modification mechanism of ZIF glasses. Addition of the halide salt partially breaks up the Zn-ligand-Zn bridges to form depolymerized structures, while further heating induces the evaporation of the linker species and subsequent formation of halide-bridged Zn centers.

In future work, the herein proposed concept for ZIF glass modification may allow for a significant enhancement of the structural diversity of MOF glasses in general. Specifically, all the systems we have tested (ZIF-4, ZIF-8, and ZIF-62 co-melted with various heterocycle cations and halide [Cl, Br, I] anions) melt and form cm-sized homogeneous glasses. Given the equivalent possibility of, e.g., carboxylate-MOFs to form mixed carboxylate-halide-node metal centers[44], we believe that the present discovery should allow for glass formation in a broad range of MOF chemistries. This would allow MOF glasses to realize the hallmark of traditional glasses, namely, the ability to tune chemical

and physical properties through continuous composition variation. We also believe that the present approach will enable new functionalities (fluorescence, sensing, etc.) of MOF glasses through the incorporation of the added salt directly into the existing framework structure.

Conclusions

We have demonstrated that the addition of an organic halide salt ("modifier") to three typical ZIF crystals results in meltable systems, which upon cooling form glasses with tunable thermal and mechanical properties depending on the composition and thermal treatment. Notably, this approach enables the melting of ZIF-8, which otherwise undergoes decomposition before melting. The approach thus provides a new paradigm for structural tuning and processing of metal-organic frameworks.

Methods

Materials. All chemicals were used as received from the supplier without further purification. $Zn(NO_3)_2 \cdot 6H_2O$ (≥99.0%), methanol (99.9%), imidazole (99.5%), benzimidazole (98%), 2-methylimidazole (99.0%), HCl (hydrochloric acid, 37%), HBr (hydrobromic acid, 48%), HI (hydriodic acid, 57 wt. % in H_2O, distilled, stabilized, 99.95%), and dimethylformamide (DMF) (99.9 %) were all acquired from Sigma-Aldrich.

Synthesis of ZIF-62 crystals. Synthesis was performed according to the procedure in Madsen *et al*.[45]. The samples were prepared by weighing zinc nitrate hexahydrate (1.7460 g), imidazole (5.3282 g), and benzimidazole (1.6268 g) and adding them sequentially to a beaker, followed by the addition of 50 mL of DMF. The solution was stirred for 30 min, then transferred to a 100 mL PTFE-lined autoclave and sealed. The mixture was then placed in an autoclave at 130 °C for 96 h. The autoclave was allowed to cool naturally in the oven to ambient temperature overnight. The synthesized crystals were recovered and washed three times with approximately 40 mL of DMF each time. The washed crystals were dried in an oven at 110 °C overnight. X-

ray diffraction results of the obtained material are presented in Fig. 1b.

Synthesis of ZIF-4 crystals. The synthesis of ZIF-4 followed the method described in Widmer *et al.*[46]. 1.2 g of $Zn(NO_3)_2 \cdot 6H_2O$ (4.03 mmol) and 0.9 g of imidazole (13.2 mmol) were dissolved in 75 mL of DMF and transferred to a 100 mL PTFE-lined autoclave and sealed. The autoclave was sealed and heated in an oven at 130 °C for 48 h. The synthesized crystals were recovered and washed three times with approximately 40 mL of DMF. The washed crystals were dried in an oven at 110 °C overnight. X-ray diffraction results of the obtained material are presented in Fig. 1b.

Synthesis of ZIF-8 crystals. ZIF-8 synthesis followed a procedure adapted from Peppel *et al.*[47]. Initially, 0.3 g of $Zn(NO_3)_2 \cdot 6H_2O$ was dissolved in 11.3 g of methanol. Subsequently, 0.66 g of 2-methylimidazole and another 11.3 g of methanol were added to the zinc-based solution. After a reaction time of 12 h, the gel formed in the solution was centrifuged at 8000 RPM to separate the crystals. The crystals were then washed three times with methanol. The washed crystals were dried at 75 °C overnight. X-ray diffraction results of the obtained material are presented in Fig. 1b.

Synthesis of benzimidazolium hydrochloride. The synthesis of benzimidazolium hydrochloride (bImCl) followed the method described by Peppel *et al.*[48]. Benzimidazole (8.671 g, 73.4 mmol) was dissolved in 25 mL demineralized water in a beaker, followed by the addition of 37% hydrochloric acid (7.95 g, 81.2 mmol) with stirring. The solutions were heated to 110℃ in an oil bath until all liquid had evaporated, resulting in the formation of white crystalline powder. The powder was dried in a vacuum environment at 110 ℃ for 24 h before being subjected to X-ray diffraction analysis as presented in Supplementary Fig. 34.

Synthesis of benzimidazolium hydrobromide. The synthesis follows the same strategy of an acid-base salt as for benzimidazolium hydrochloride. Benzimidazole (8.671 g, 73.4 mmol) was dissolved in 25 mL demineralized water in a beaker, followed by the addition of 48%

hydrobromic acid (13.686 g, 81.2 mmol) with stirring. The solutions were heated to 110 °C in an oil bath until all liquid had evaporated, resulting in the formation of brown crystalline powder. The powder was dried in a vacuum environment at 110 °C for 24 h before being subjected to X-ray diffraction analysis as presented in Supplementary Fig. 34.

Synthesis of benzimidazolium hydriodate. The synthesis follows the same strategy of and acid-base salt as for benzimidazolium hydrochloride. Benzimidazole (8.671 g, 73.4 mmol) was dissolved in 25 mL demineralized water in a beaker, followed by the addition of 57% hydriodic acid (18.222 g, 81.2 mmol) with stirring. The solutions were heated to 110 ℃ in an oil bath until all liquid had evaporated, resulting in the formation of gray-black crystalline powder. The powder was dried in a vacuum environment at 110 ℃ for 24 h before being subjected to X-ray diffraction analysis as presented in Supplementary Fig. 34.

Preparation of modified ZIF glasses. The utilized heating source was a hotplate (IKA C-MAG HS7 hotplate stirrer), upon which an aluminum block with drilled holes was positioned to ensure uniform heating of the quartz test tube (see Supplementary Fig. 35 for an illustration of the setup). Approximately 0.2 g of ZIF crystal and varying amounts of salt (depending on the desired molar ratio *R*) were accurately weighed, and then ground using a mortar and pestle to achieve a homogeneous mixture. The mixture was subsequently transferred into the test tube, which was sealed with a soft plug. Argon gas was purged into the test tube to remove any air, and then the test tube was placed in the preheated aluminum block at a predetermined temperature for heating and melting of the mixture. Finally, the test tube was cooled to room temperature to obtain the hybrid glass by simply removing the quartz tube from the aluminum block.

Fast scanning differential calorimetry. All fast scanning differential calorimetry (FDSC) measurements were done using a Mettler Toledo Flash DSC 2+ device. Samples were initially crushed under a scalpel blade. For each sample, a single grain (microgram range) of the homogenous sample was loaded onto the active area of a Mettler Toledo pre-conditioned and

pre-corrected UFS1 sensor using a hair (see example of a loaded sample in Supplementary Fig. 36). The sample was then prepared at temperatures ranging from 200-300 °C i.e., well above T_g of the modified ZIF glasses, to establish a good thermal contact between the sensor and the sample. All sample scans were performed in a nitrogen atmosphere (flow of 20 mL min^{-1}). The presented FDSC results are shown uncorrected. Glass transition temperatures are reported as onset temperatures, i.e. the intersection between the extrapolated lines of the heat flow in the glassy state (significantly below T_g) and the tangent of the inflection point of the glass transition peak.

Standard differential scanning calorimetry. Standard differential scanning calorimetry measurements were performed using a Netzsch STA F449 F3 instrument equipped with liquid N_2 cooling. Measurements were performed in a Netzsch cold-welded aluminum crucible in a He atmosphere. Heating and cooling rates of 10 K min^{-1} were used. The thermal history of the measured glass was 'reset' by heating to 200 °C (i.e., >>T_g) before cooling at a rate of 10 K min^{-1} and finally acquiring a heating scan at 10 K min^{-1}.

X-ray diffraction. X-ray diffraction (XRD) measurements of the samples were performed on a PANalytical Empyrean X-ray diffractometer with Cu Kα (λ=1.5406 Å) radiation. The XRD patterns were collected in the 2θ range of 5-40° with a step size of 0.013°.

X-ray total scattering. X-ray total scattering measurements were conducted at the P02.1 beamline at PETRA III, Deutsches Elektronen-Synchrotron (DESY) in Hamburg, Germany. The data were collected on an amorphous silicon two-dimensional flat panel Varex XRD 4343CT (2880×2880 pixel matrix for 150×150 μm^2 pixel size) in corner configuration with a quarter ring Q_{max} of 28.1 $Å^{-1}$. The beam spot was 1×1 mm^2 and the used wavelength λ was 0.207 Å (~60 keV). *In situ* temperature-resolved measurements were performed in quartz glass capillaries (QGCT 1.0, Capillary Tube Supplies Ltd) with an inner diameter of 0.9 mm and a 0.1 mm wall thickness, whereas the glass samples measured *ex situ* at room temperature were placed in Kapton capillaries (Cole-Parmer Instrument Company, Polyimide tubing 1.2 mm)

with an inner diameter of 1.03 mm and a 0.051 mm wall thickness to achieve good transmission of X-rays. The *in situ* measurements were performed using an exposure time of 60 s at each 10 K temperature step. Heating and cooling between steps were performed at a ramp of 25 K min^{-1} using a hot air blower[49]. Real and setpoint temperatures were checked using the (2 0 0) Bragg reflection of a copper sample. We found a difference between real and setpoints temperatures of <10 K (Supplementary Figs. 37-38) for all measurements and we thus used the setpoint temperature for all reported temperatures of the total scattering data. The *ex situ* measurements were performed at room temperature using an exposure time of 600 s.

To process the obtained data, azimuthal integration and calibration were made using pyFAI[50] software. LaB_6 was used as calibrant for the detector to sample distance and angle. xPDFsuite[51] was used for subtraction of the empty quartz glass and Kapton capillaries integration intensities and to obtain the $S(Q)$ (R_{poly}=1.20). The Fourier transform was made over the Q-range of 0.1 to 20 $Å^{-1}$ of the reduced total scattering structure function ($F(Q) = Q[S(Q) - 1]$) as obtained from xPDFsuite. This procedure was performed using an in-house code. A Lorch window function[52] (with Q_{max}=20 $Å^{-1}$) was used to process the *ex situ* data (Fig. 3c,d) to reduce the effect of termination ripples in the resulting $G(r)$ from the Fourier transform. All *in situ* data (Fig. 3b and all PDFs in the Supplementary Information) are presented without the use of a Lorch function.

X-ray photoelectron spectroscopy. Before each X-ray photoelectron spectroscopy (XPS) measurement, the glass samples were polished using SiC paper with anhydrous diamond suspension and hexane to obtain a smooth surface. The crystalline samples were dried and ground into powder using a mortar. The XPS measurements were performed using a Hiden MAXIM SIMS system equipped with a Specs XR50 X-ray source and a Specs Phoibos 150 electronic analyzer. The X-ray beam generated by the aluminum anode had a wavelength of λ=0.83401 nm, and X-ray optics ensured signal collection from spots approximately 2 mm in diameter, including glass samples. Subsequent data analysis was performed using CasaXPS software, involving standard energy correction and background removal procedures based on the expected C1s transition (284.8 eV).

Raman spectroscopy. Micro-Raman spectra were recorded with a diode laser of 532 nm wavelength equipped on a Renishaw Invia spectroscope.

Fourier transform infrared spectroscopy. FTIR spectra were recorded using an attenuated total reflection setup on a Bruker Tensor II spectrometer. Crystalline diamond was used as the attenuation crystal. All samples were measured under ambient conditions in the 400-4000 cm^{-1} frequency range.

Solid-state ^{1}H MAS NMR

Solid-state ^{1}H MAS NMR analyses were carried out on a 22.3 T Bruker Avance NEO (950 MHz for ^{1}H) spectrometer equipped with 1.9 mm HCND four-channel probe. Direct pulse MAS (35 kHz spinning frequency) experiments (single 90-degree pulse; pulse length/amplitude 4 μs/50 kHz; 3 s repetition delay; 16 scans) were used for acquiring the experimental data. The isotropic chemical shifts are relative to ^{1}H signal for adamantane (1.82 ppm).

Solid-state ^{13}C MAS NMR

Solid-state ^{13}C MAS NMR analyses were carried out on a 16.4 T Bruker Avance III HD wide-bore (700 MHz for ^{1}H) spectrometer equipped with 4 mm HXY triple-resonance probe in double-resonance mode at MAS frequency of 15 kHz. ^{1}H-^{13}C Cross-Polarization were used for acquiring experimental data using a field strength of 64 kHz on ^{1}H and 50 kHz on ^{13}C with a 80-100% RAMP on ^{1}H channel (contact period of 0.75 ms). ^{1}H decoupling (SPINAL64, 110 kHz) was employed during the free acquisition time. Spectra were recorded using a repetition delay of 3 s. A total number of 312 scans (ZIF-62 glass) and 912 scans (ZIF-62-bImCl R=1 glass) were acquired. The isotropic chemical shifts are relative to ^{13}C signal for adamantane (37.8 ppm).

Solid-state ^{15}N MAS NMR

Solid-state ^{15}N MAS NMR analyses were carried out on a 16.4 T Bruker Avance III HD wide-

bore (700 MHz for ^{1}H) spectrometer equipped with 4 mm HXY triple-resonance probe in double-resonance mode at MAS frequency of 15 kHz. ^{1}H-^{15}N Cross-Polarization were used for acquiring experimental data using a field strength of 35 kHz on ^{1}H (with 80-100% RAMP) and 18 kHz on ^{15}N channel (contact time of 10 ms). ^{1}H decoupling (SPINAL64, 110 kHz) was employed during the free acquisition time. ZIF-62 glass spectra used a repetition delay of 2 s and were recorded using 4096 scans. For the ZIF-62-bImCl *R*=1 glass, spectra a repetition delay of 5 s and 45769 scans were acquired. The isotropic chemical shifts are relative to a solid sample of NH_4Cl set to 39.3 ppm.

Solid-state ^{67}Zn MAS NMR

Solid-state ^{67}Zn MAS NMR analyses were carried out on a 22.3 T Bruker Avance NEO (950 MHz for ^{1}H) spectrometer equipped with 4 mm HX double-resonance probe at MAS frequency of 15 kHz. The data were recorded using a Hahn-echo pulse sequence using 17 kHz rf field strength with a total echo-time of one rotor period (lengths of 2 and 4 μs for the π/2 and π pulses, respectively). The spectra used a repetition delay of 0.1 s. In addition, an empty rotor experiment was recorded and subtracted. The isotropic chemical shifts are relative to an aqueous 1.0 M solution of $Zn(NO_3)_2$.

Scanning electron microscopy and energy dispersive X-ray analysis. The samples were directly placed onto the conductive adhesive and then sprayed with gold for 45 seconds using a Quorum SC7620 sputter coater at 10 mA. The microstructures of the samples were then acquired using a ZEISS GeminiSEM 300 scanning electron microscope for topography and energy mapping, with an accelerating voltage of 3 kV for topography and 15 kV for energy mapping. The detector was an SE2 secondary electron detector.

Micro indentation. Vickers hardness (H_V) and crack initiation resistance (CR) of the samples were measured by micro-indentation (CB500, Nanovea). For hardness tests, we used a Vickers diamond tip (four-sided pyramid-shaped diamond with an angle of 136° between opposing faces) to produce indents at varying peak loads on each sample, with a loading speed of 0.05 N

min^{-1} and a holding time of 6 s. 15 indents were analyzed for each sample. The lengths of the two indent diagonals were measured using an optical microscope. H_V was then calculated as,

$$H_V = \frac{0.1891P}{d^2},$$

where P is the used indentation force and d is the average indent diagonal length. The CR value corresponds to the load value with a probability of corner cracking of 50%[53]. Specifically, the initiation probability of crack initiation is defined as the ratio between the number of cracked corners and the total number of corners during the test. The measurement of CR was also done using the Vickers tip, but here we used varying peak loads. The number of corners with cracks after unloading at different loads and different loading rates were observed using a microscope. The indentations were performed under laboratory conditions (23 °C, ~40% relative humidity). The ratio between the number of cracked corners and the total number of corners was recorded for each load 1 h after unloading. For each sample and load, 15 indents were analyzed.

Ab initio molecular dynamics simulations. We performed ab initio molecular dynamics (AIMD) simulations of a unit cell of ZIF-62 including eight structures of added benzimidazolium chloride. The initial structure was made using packmol, where benzimidazolium and chloride were placed randomly in a crystalline unit cell of ZIF-62 while keeping a minimum distance of 2 Å to the existing atoms. The dynamics simulations were then performed with the Vienna Ab initio Simulation Package (VASP) using the standard PBE pseudopotential and a time step of 0.5 fs. An energy cutoff of 400 eV and a convergence criterion of 10^{-4} eV was used. First, the structure was relaxed while allowing relaxation of both unit cell dimensions and positions using a target pressure of 0. Next, dynamics were initiated at 1000 K and run for 10 ps (a total of 20,000 molecular dynamics steps). In this process, the structure was allowed to deform freely with a target pressure of 0.

Author contributions

S.S.S. conceived the idea of the project. F.C., S.S.S., and M.M.S. planned the study. F.C. performed all sample synthesis, XRD, FTIR, SEM, and EDX measurements and analyses. S.S.S.

performed atomistic simulations. S.S.S., F.D., J.B., G.M., and F.C. performed calorimetric measurements and analyses. P.K.K. performed XPS measurements and analyses. L.R.J. and F.C. performed Raman spectroscopy measurements and analyses. A.B.N. and N.C.N. performed solid-state NMR measurements and analyses. A.K.R.C., S.S.S., F.C., S.M., M.A.K., V.B., and X.G. performed X-ray synchrotron measurements and analyses. F.C. and D.S. performed the micro indentation experiments and analyses. X.G. participated in part of the experimental design. S.S.S. and M.M.S. supervised the study. F.C., S.S.S., and M.M.S. wrote the manuscript, with input from all other authors. All authors discussed the results.

Acknowledgements

We acknowledge M. Umair and L. Piemontese (University of Padova) for assistance with calorimetry measurements and N. Bjerre-Christensen and D. Ravnsbæk (Aarhus University) for preliminary X-ray total scattering measurements. M.M.S. acknowledges support from the European Union (ERC, NewGLASS, 101044664), the ESS lighthouse on hard materials in 3D, SOLID, funded by the Danish Agency for Science and Higher Education (8144-00002), and Independent Research Fund Denmark (grant no. 1127-00003). Views and opinions expressed are however those of the author(s) only and do not necessarily reflect those of the European Union or the European Research Council. Neither the European Union nor the granting authority can be held responsible for them. F.C. acknowledges support from the China Scholarship Council (202206890034). N.C.N. and A.B.N. acknowledge support from the Novo Nordisk Foundation NERD program (NNF22OC0076002) and the use of NMR facilities at the Danish Center for Ultrahigh-Field NMR Spectroscopy funded by the Danish Ministry of Higher Education and Science (AU-2010-612-181) and Novo Nordic Foundation Research Infrastructure – Large Equipment and Facilities (NNF220C0075797). We acknowledge DESY (Hamburg, Germany), a member of the Helmholtz Association HGF, for the provision of experimental facilities and travel support. Parts of this research were carried out at PETRA III beamline P02.1. Beamtime was allocated for proposal I-20230857 EC. We acknowledge the Danish Agency for Science, Technology, and Innovation for travel funding through DanScatt.

We acknowledge the computational resources supplied by Aalborg University (through CLAAUDIA) and through access to the LUMI HPC through DeiC (grant no. DeiC-AAU-N5-000006) as well as funding from the Carlsberg Foundation (CF21-0371) for the standard DSC instrument.

References

1. Varshneya AK, Mauro JC. *Fundamentals of Inorganic Glasses (Third Edition)*. Elsevier, 2019.

2. Liu M, Slavney AH, Tao S, McGillicuddy RD, Lee CC, Wenny MB*, et al.* Designing Glass and Crystalline Phases of Metal–Bis(acetamide) Networks to Promote High Optical Contrast. *Journal of the American Chemical Society* 2022, **144**(48)**:** 22262-22271.

3. Lee J, Farha OK, Roberts J, Scheidt KA, Nguyen ST, Hupp JT. Metal-organic framework materials as catalysts. *Chem Soc Rev* 2009, **38**(5)**:** 1450-1459.

4. Moghadam PZ, Li A, Wiggin SB, Tao A, Maloney AGP, Wood PA*, et al.* Development of a Cambridge Structural Database Subset: A Collection of Metal–Organic Frameworks for Past, Present, and Future. *Chemistry of Materials* 2017, **29**(7)**:** 2618-2625.

5. Smirnova O, Hwang S, Sajzew R, Ge L, Reupert A, Nozari V*, et al.* Precise control over gas-transporting channels in zeolitic imidazolate framework glasses. *Nature Materials* 2024, **23**(2)**:** 262-270.

6. Wei T, Wang Z, Zhang Q, Zhou Y, Sun C, Wang M*, et al.* Metal–organic framework-based solid-state electrolytes for all solid-state lithium metal batteries: a review. *CrystEngComm* 2022, **24**(28)**:** 5014-5030.

7. Farha OK, Eryazici I, Jeong NC, Hauser BG, Wilmer CE, Sarjeant AA*, et al.* Metal-organic framework materials with ultrahigh surface areas: is the sky the limit? *J Am Chem Soc* 2012, **134**(36)**:** 15016-15021.

8. Horike S, Shimomura S, Kitagawa S. Soft porous crystals. *Nature Chemistry* 2009, **1**(9)**:** 695-704.

9. Furukawa H, Cordova KE, O'Keeffe M, Yaghi OM. The chemistry and applications of metal-organic frameworks. *Science* 2013, **341**(6149)**:** 1230444.

10. Stepniewska M, Østergaard MB, Zhou C, Yue Y. Towards large-size bulk ZIF-62 glasses via optimizing the melting conditions. *Journal of Non-Crystalline Solids* 2020, **530:**

119806.

11. Zheng Q, Mauro JC. Viscosity of glass-forming systems. *Journal of the American Ceramic Society* 2016, **100**(1)**:** 6-25.

12. Nozari V, Calahoo C, Tuffnell JM, Keen DA, Bennett TD, Wondraczek L. Ionic liquid facilitated melting of the metal-organic framework ZIF-8. *Nat Commun* 2021, **12**(1)**:** 5703.

13. Yaghi OM. Evolution of MOF single crystals. *Chem* 2022, **8**(6)**:** 1541-1543.

14. Bennett TD, Horike S. Liquid, glass and amorphous solid states of coordination polymers and metal–organic frameworks. *Nature Reviews Materials* 2018, **3**(11)**:** 431-440.

15. Jain A, Ong SP, Hautier G, Chen W, Richards WD, Dacek S*, et al.* Commentary: The Materials Project: A materials genome approach to accelerating materials innovation. *APL Materials* 2013, **1:** 011002.

16. Jiusti J, Zanotto ED, Feller SA, Austin HJ, Detar HM, Bishop I*, et al.* Effect of network formers and modifiers on the crystallization resistance of oxide glasses. *Journal of Non-Crystalline Solids* 2020, **550:** 120359.

17. Liu Q, Miao Y, Villalobos LF, Li S, Chi H-Y, Chen C*, et al.* Unit-cell-thick zeolitic imidazolate framework films for membrane application. *Nature Materials* 2023, **22**(11)**:** 1387-1393.

18. Du Z, Qiao A, Zhou H, Li Z, Winters WMW, Zhu J*, et al.* The glass transition in the high-density amorphous Zn/Co-ZIF-4. *Chem Commun (Camb)* 2023, **59**(79)**:** 11871-11874.

19. Li S, Limbach R, Longley L, Shirzadi AA, Walmsley JC, Johnstone DN*, et al.* Mechanical Properties and Processing Techniques of Bulk Metal-Organic Framework Glasses. *J Am Chem Soc* 2019, **141**(2)**:** 1027-1034.

20. Gaillac R, Pullumbi P, Beyer KA, Chapman KW, Keen DA, Bennett TD*, et al.* Liquid metal–organic frameworks. *Nature Materials* 2017, **16**(11)**:** 1149-1154.

21. Gaillac R, Pullumbi P, Coudert F-X. Melting of Zeolitic Imidazolate Frameworks with Different Topologies: Insight from First-Principles Molecular Dynamics. *The Journal of Physical Chemistry C* 2018, **122**(12)**:** 6730-6736.

22. Frentzel-Beyme L, Kloss M, Kolodzeiski P, Pallach R, Henke S. Meltable Mixed-Linker Zeolitic Imidazolate Frameworks and Their Microporous Glasses: From Melting Point Engineering to Selective Hydrocarbon Sorption. *J Am Chem Soc* 2019, **141**(31)**:** 12362-12371.

23. León-Alcaide L, Christensen RS, Keen DA, Jordá JL, Brotons-Alcázar I, Forment-Aliaga A*, et al.* Meltable, Glass-Forming, Iron Zeolitic Imidazolate Frameworks. *Journal of the American Chemical Society* 2023, **145**(20)**:** 11258-11264.

24. Sørensen SS, Christensen AKR, Bouros-Bandrabur EA, Andersen ES, Christiansen HF, Lang S*, et al.* Water Promotes Melting of a Metal–Organic Framework. *Chemistry of Materials* 2024, **36**(6)**:** 2756-2766.

25. Deubener J, Müller R, Behrens H, Heide G. Water and the glass transition temperature of silicate melts. *Journal of Non-Crystalline Solids* 2003, **330**(1-3)**:** 268-273.

26. Mroué KH, Power WP. High-Field Solid-State 67Zn NMR Spectroscopy of Several Zinc−Amino Acid Complexes. *The Journal of Physical Chemistry A* 2010, **114**(1)**:** 324-335.

27. Lundberg B. The crystal structure of di-imidazole-zinc(II) dichloride. *Acta Crystallographica* 1966, **21**(6)**:** 901-909.

28. Bumstead AM, Pakamore I, Richards KD, Thorne MF, Boyadjieva SS, Castillo-Blas C*, et al.* Post-Synthetic Modification of a Metal-Organic Framework Glass. *Chem Mater* 2022, **34**(5)**:** 2187-2196.

29. Bumstead AM, Ríos Gómez ML, Thorne MF, Sapnik AF, Longley L, Tuffnell JM*, et al.* Investigating the melting behaviour of polymorphic zeolitic imidazolate frameworks. *CrystEngComm* 2020, **22**(21)**:** 3627-3637.

30. Bennett TD, Yue Y, Li P, Qiao A, Tao H, Greaves NG*, et al.* Melt-Quenched Glasses of Metal-Organic Frameworks. *J Am Chem Soc* 2016, **138**(10)**:** 3484-3492.

31. Stepniewska M, Januchta K, Zhou C, Qiao A, Smedskjaer MM, Yue Y. Observation of indentation-induced shear bands in a metal-organic framework glass. *Proceedings of the National Academy of Sciences* 2020, **117**(19)**:** 10149-10154.

32. To T, Sorensen SS, Stepniewska M, Qiao A, Jensen LR, Bauchy M*, et al.* Fracture toughness of a metal-organic framework glass. *Nat Commun* 2020, **11**(1)**:** 2593.

33. Qiao A, To T, Stepniewska M, Tao H, Calvez L, Zhang X*, et al.* Deformation mechanism of a metal–organic framework glass under indentation. *Physical Chemistry Chemical Physics* 2021, **23**(31)**:** 16923-16931.

34. Gong Y, Zhang H, Li P, Bai Y, Yin B, Ouyang M*, et al.* Spectral and Temporal Manipulation of Ultralong Phosphorescence Based on Melt-Quenched Glassy Metal–Organic Complexes for Multi-Mode Photonic Functions. *Advanced Functional Materials* 2024, **34**(23)**:** 2312491.

35. Qiao A, Bennett TD, Tao H, Krajnc A, Mali G, Doherty CM*, et al.* A metal-organic framework with ultrahigh glass-forming ability. *Science Advances* 2018, **4**(3)**:** eaao6827.

36. Bak M, Rasmussen JT, Nielsen NC. SIMPSON: A General Simulation Program for Solid-State NMR Spectroscopy. *Journal of Magnetic Resonance* 2000, **147**(2)**:** 296-330.

37. Madsen RSK, Qiao A, Sen J, Hung I, Chen K, Gan Z*, et al.* Ultrahigh-field 67Zn NMR reveals short-range disorder in zeolitic imidazolate framework glasses. *Science* 2020, **367**(6485)**:** 1473-1476.

38. Ueda T, Nagatomo S, Masui H, Nakamura N, Hayashi S. Hydrogen Bonds in Crystalline Imidazoles Studied by 15N NMR and ab initio MO Calculations. *Zeitschrift für Naturforschung A* 1999, **54**(6-7)**:** 437-442.

39. Song X-j, McDermott AE. Proton transfer dynamics and N—H bond lengthening in N—H···N model systems: a solid-state NMR study. *Magnetic Resonance in Chemistry* 2001, **39**(S1)**:** S37-S43.

40. Nieto CI, Cabildo P, García MÁ, Claramunt RM, Alkorta I, Elguero J. An experimental and theoretical NMR study of NH-benzimidazoles in solution and in the solid state: proton transfer and tautomerism. *Beilstein Journal of Organic Chemistry* 2014, **10:** 1620-1629.

41. Maeda M, Ito T, Hori M, Johansson G. The Structure of Zinc Chloride Complexes in Aqueous Solution. 1996, **51**(1-2)**:** 63-70.

42. Wakita H, Johansson G, Sandström M, Goggin PL, Ohtaki H. Structure determination of zinc iodide complexes formed in aqueous solution. *Journal of Solution Chemistry* 1991, **20**(7)**:** 643-668.

43. Goggin PL, Johansson G, Maeda M, Wakita H. The Structures of Zinc Bromide Complexes in Aqueous Solution. *Acta Chemica Scandinavica A* 1984, **38**(8)**:** 625-639.

44. Chen X, Peng C, Dan W, Yu L, Wu Y, Fei H. Bromo- and iodo-bridged building units in metal-organic frameworks for enhanced carrier transport and CO(2) photoreduction by water vapor. *Nat Commun* 2022, **13**(1)**:** 4592.

45. Madsen RSK, Sarkar S, Iversen BB, Yue Y. Sensitivity of the glass transition and melting in a metal–organic framework to ligand chemistry. *Chemical Communications* 2022, **58**(6)**:** 823-826.

46. Widmer RN, Lampronti GI, Anzellini S, Gaillac R, Farsang S, Zhou C*, et al.* Pressure promoted low-temperature melting of metal-organic frameworks. *Nat Mater* 2019, **18**(4)**:** 370-376.

47. Venna SR, Jasinski JB, Carreon MA. Structural Evolution of Zeolitic Imidazolate Framework-8. *Journal of the American Chemical Society* 2010, **132**(51)**:** 18030-18033.

48. Peppel T, Roth C, Fumino K, Paschek D, Kockerling M, Ludwig R. The influence of hydrogen-bond defects on the properties of ionic liquids. *Angew Chem Int Ed Engl* 2011, **50**(29)**:** 6661-6665.

49. Dippel A-C, Liermann H-P, Delitz JT, Walter P, Schulte-Schrepping H, Seeck OH*, et al.* Beamline P02.1 at PETRA III for high-resolution and high-energy powder diffraction. *Journal of Synchrotron Radiation* 2015, **22**(3)**:** 675-687.

50. Kieffer J, Valls V, Blanc N, Hennig C. New tools for calibrating diffraction setups. *Journal of Synchrotron Radiation* 2020, **27**(2)**:** 558-566.

51. Yang X, Juhas P, Farrow CL, Billinge SJL. xPDFsuite: an end-to-end software solution for high throughput pair distribution function transformation, visualization and analysis. *Arxiv: cond-mat: Materials Science* 2015**:** 1402.3163v1403

52. Lorch E. Neutron diffraction by germania, silica and radiation-damaged silica glasses. *Journal of Physics C: Solid State Physics* 1969, **2**(2)**:** 229.

53. Januchta K, Smedskjaer MM. Indentation deformation in oxide glasses: Quantification, structural changes, and relation to cracking. *Journal of Non-Crystalline Solids: X* 2019, **1:** 100007.